Volume 6 | Number 2 | February 2014 | Pages 103–234

Integrative Biology

Interdisciplinary approaches for molecular and cellular life sciences

www.rsc.org/ibiology

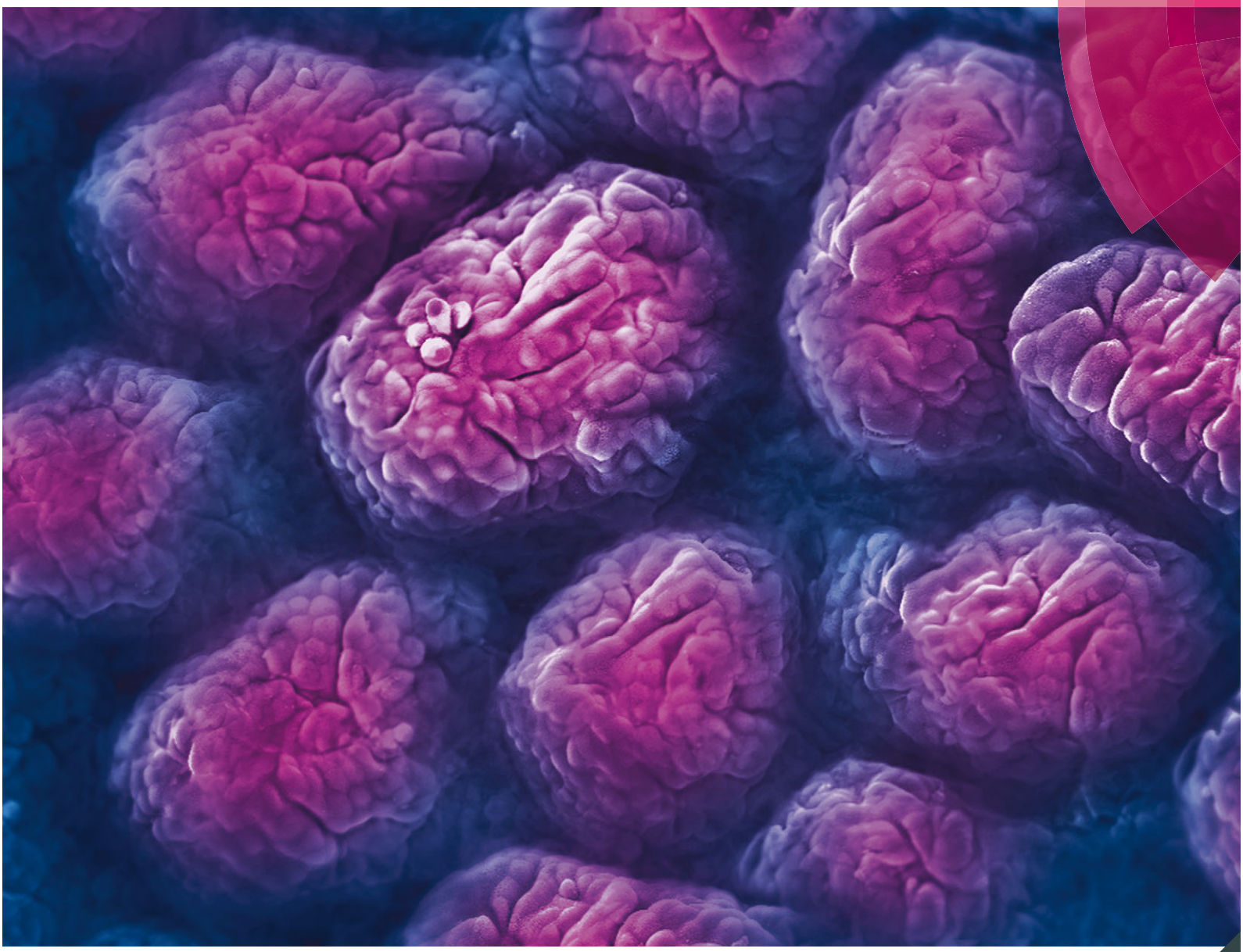

ISSN 1757-9694

ROYAL SOCIETY OF CHEMISTRY

PAPER
Sarah C. Heilshorn *et al.*
Engineering of three-dimensional microenvironments to promote contractile behavior in primary intestinal organoids

Indexed in Medline!

Integrative Biology

PAPER

Engineering of three-dimensional microenvironments to promote contractile behavior in primary intestinal organoids†

Cite this: *Integr. Biol.*, 2014, **6**, 127

Rebecca L. DiMarco,‡[a] James Su,‡[b] Kelley S. Yan,[c] Ruby Dewi,[b] Calvin J. Kuo[c] and Sarah C. Heilshorn*[b]

Received 14th September 2013,
Accepted 21st November 2013

DOI: 10.1039/c3ib40188j

www.rsc.org/ibiology

Multiple culture techniques now exist for the long-term maintenance of neonatal primary murine intestinal organoids *in vitro*; however, the achievement of contractile behavior within cultured organoids has thus far been infrequent and unpredictable. Here we combine finite element simulation of oxygen transport and quantitative comparative analysis of cellular microenvironments to elucidate the critical variables that promote reproducible intestinal organoid contraction. Experimentally, oxygen distribution was manipulated by adjusting the ambient oxygen concentration along with the use of semi-permeable membranes to enhance transport. The culture microenvironment was further tailored through variation of collagen type-I matrix density, addition of exogenous R-spondin1, and specification of culture geometry. "Air–liquid interface" cultures resulted in significantly higher numbers of contractile cultures relative to traditional submerged cultures. These interface cultures were confirmed to have enhanced and more symmetric oxygen transport relative to traditional submerged cultures. While oxygen availability was found to impact *in vitro* contraction rate and the orientation of contractile movement, it was not a key factor in enabling contractility. For all conditions tested, reproducible contractile behavior only occurred within a consistent and narrow range of collagen type-I matrix densities with porosities of approximately 20% and storage moduli near 30 Pa. This suggests that matrix density acts as a "permissive switch" that enables contractions to occur. Similarly, contractions were only observed in cultures with diameters less than 15.5 mm that had relatively large interfacial surface area between the compliant matrix and the rigid culture dish. Taken together, these data suggest that spatial geometry and mechanics of the microenvironment, which includes both the encapsulating matrix as well as the surrounding culture device, may be key determinants of intestinal organoid functionality. As peristaltic contractility is a crucial requirement for normal digestive tract function, this achievement of reproducible organoid contraction marks a pivotal advancement towards engineering physiologically functional replacement tissue constructs.

Insight, innovation, integration

Through engineering of the cell culture microenvironment, we achieved reproducible contraction of encapsulated primary murine intestinal organoids with tunable rate and direction of contractile movement *in vitro*. The *Technological Innovation* included combined use of an air–liquid interface culture system together with variable atmospheric oxygen and finite element modeling to exert control over the oxygen concentration profile within the three-dimensional cultures. The *Integration* of matrix characterization, three-dimensional organoid cell culture, and computational simulation enabled *Biological Insight* into the matrix parameters that permit organoid contraction and the distinct roles of oxygen in influencing organoid contractile behavior. Achieving reliable, reproducible contractions of intestinal organoids *in vitro* is a critical advancement towards the engineering of physiologically functional tissue for drug screening assays, models of intestinal diseases, and potential regenerative medicine therapies.

[a] *Department of Bioengineering, Stanford University, Stanford, CA, USA*
[b] *Department of Materials Science and Engineering, Stanford University, Stanford, CA, USA. E-mail: heilshorn@stanford.edu; Fax: +1-650-498-5596; Tel: +1-650-723-3763*
[c] *Department of Medicine, Hematology Division, Stanford University School of Medicine, Stanford, CA, USA*

† Electronic supplementary information (ESI) available. See DOI: 10.1039/c3ib40188j

‡ These authors contributed equally to this work.

Introduction

Intestinal diseases, such as necrotizing enterocolitis, inflammatory bowel diseases, and gastrointestinal cancers, can require resection of the afflicted intestinal tissue as a means of treatment.[1,2] In severe cases, this results in a loss of the ability to properly digest food and absorb necessary nutrients; thus, patient

survival requires either an intestinal transplant or the lifelong dependency on intravenously administered nutrition.[1–4] Intestinal transplantation is plagued by high morbidity, low supply of healthy tissue, and side effects of chronic immunosuppression, whereas intravenous nutritional support greatly diminishes quality of life and has long-term risks of infection, eventual loss of venous access, and subsequent liver failure.[4–11]

Tissue engineering is a promising strategy for intestinal tissue replacement. To date, intestinal regeneration efforts have primarily focused on the use of gastrointestinal-derived submucosa, abdominal wall, or peritoneal ''patches'' to promote localized healing.[4,12–15] Though some of these techniques result in successful tissue regeneration in animal models, their utility is typically limited to the repair of punctate regions of afflicted tissue rather than large-scale tissue replacement.

Until recently, efforts to engineer replacement tissue constructs have been thwarted by a lack of successful long-term *in vitro* culture techniques for primary intestinal cells, although short-term maintenance of intestinal epithelial cultures was reported in the early 1990's.[16] In contrast, *in vivo* cultures in which the host omentum is used as a bioreactor have demonstrated gastrointestinal organoid fusion into tubular tissue constructs suitable for transplantation in various animal models.[3,17–21] These influential studies have demonstrated that, given the proper culture conditions, gastrointestinal tissue can be regenerated from multiple individual organoid cultures, though this has yet to be demonstrated *in vitro*.

In 2009, two distinct culture techniques were published that enable long-term *in vitro* maintenance of primary neonatal murine intestinal organoids.[22,23] These methods differ in media formulation, population of included cell types, and structural configuration of the culture-setup. In one method, isolated intestinal crypts are encapsulated within matrigel, seeded onto the bottom of a culture dish, and submerged in moderately supplemented medium.[23] In the alternative method, minced tissue sections containing both epithelial and supportive stromal cells are encapsulated within a collagen matrix and seeded onto a suspended porous transwell insert.[22] A minimally supplemented culture medium is then placed in the well surrounding, but not inside of, the main transwell insert compartment. The insert thus serves to maintain the organoids at a height that is roughly equivalent to that of the air–liquid interface surrounding the insert. The organoid-containing matrix is thereby exposed to open-air conditions, and nutrient diffusion from the medium can only occur in a bottom-up fashion through the porous membrane. Under both culture set-ups, lumen-containing, spheroid-like organoids develop from cell clusters isolated from primary neonatal murine intestinal tissue.

The success of these two distinctly different culture techniques has prompted discussion in the field regarding the importance of various culture parameters in promoting primary intestinal cell survival and functionality *in vitro*.[24] Towards elucidating these critical culture parameters, our study represents the first systematic approach at probing how *in vitro* microenvironmental cues impact the functional behavior of primary intestinal organoids. A better understanding of these critical parameters will be necessary to adapt these techniques to culture human primary intestinal cells. Thus far, *in vitro* culture of primary human intestinal organoids isolated from healthy tissue requires the addition of Wnt3A, nicotinamide, a small molecule ALK4/5/7 inhibitor (A83-01), and a p38 inhibitor (SB202190).[25] The establishment of successful culture conditions that more closely resemble a healthy native state is necessary in moving towards the *in vitro* regeneration of a replacement construct that can perform the necessary physiologic functions of normal tissue.

In this work, strategic engineering of the *in vitro* microenvironment was utilized to promote contractile behavior of primary intestinal organoids. Proper gastrointestinal function requires tissue contraction to achieve segmentation and peristalsis. *In vitro* contraction of primary intestinal organoids has thus far been a rare occurrence briefly mentioned in literature and has only been noted for organoid cultures containing stromal myofibroblasts.[22] Contractile behavior has not been reported for purified crypt populations or for isolated intestinal myofibroblasts when cultured individually. This strongly suggests that a multicellular system containing both epithelial cells as well as myofibroblasts is needed to achieve contractile behavior *in vitro*; therefore, for the purpose of our study, we chose to investigate the role of culture parameters on organoid cultures that contain both of these crucial cell types. In an effort to promote contractility of organoids, we systematically investigated the effects of exogenous Wnt signaling, collagen matrix density, oxygen transport properties, and ambient oxygen concentration within engineered microenvironments.

By studying these culture parameters in a detailed, systematic manner, we have developed a culture protocol through which organized contractions are repeatedly seen in nearly 10% of cultured organoids, a similar reproducibility as that reported for iPSC-derived epithelial-cyst-like structures and smooth muscle sheets.[26] Though additional culture characterization is needed to more fully recreate an intestinal niche-like environment, achieving reproducible organoid contraction is a pivotal advancement in moving towards physiologically functional, engineered replacement tissue constructs.

Results

Organoid formation in submerged and air–liquid interface culture configurations

Minced tissue explants were harvested and seeded within a collagen matrix according to established protocol to achieve formation of intestinal organoids.[22] *In vitro* intestinal organoids are spheroid-like structures that self-organize from primary tissue explants into lumen-enclosing epithelial layers that are surrounded by intestinal myofibroblast networks (Fig. 1). The cellular collagen gels were cast in either a typical, petri dish submerged-type configuration or on the top of a semi-permeable membrane within a transwell insert (air–liquid interface) (Fig. 2). It is important to note that the submerged organoid cultures studied in this work include stromal myofibroblasts, which is a significant difference compared to previously reported work on submerged cultures of intestinal crypts without myofibroblasts.[23]

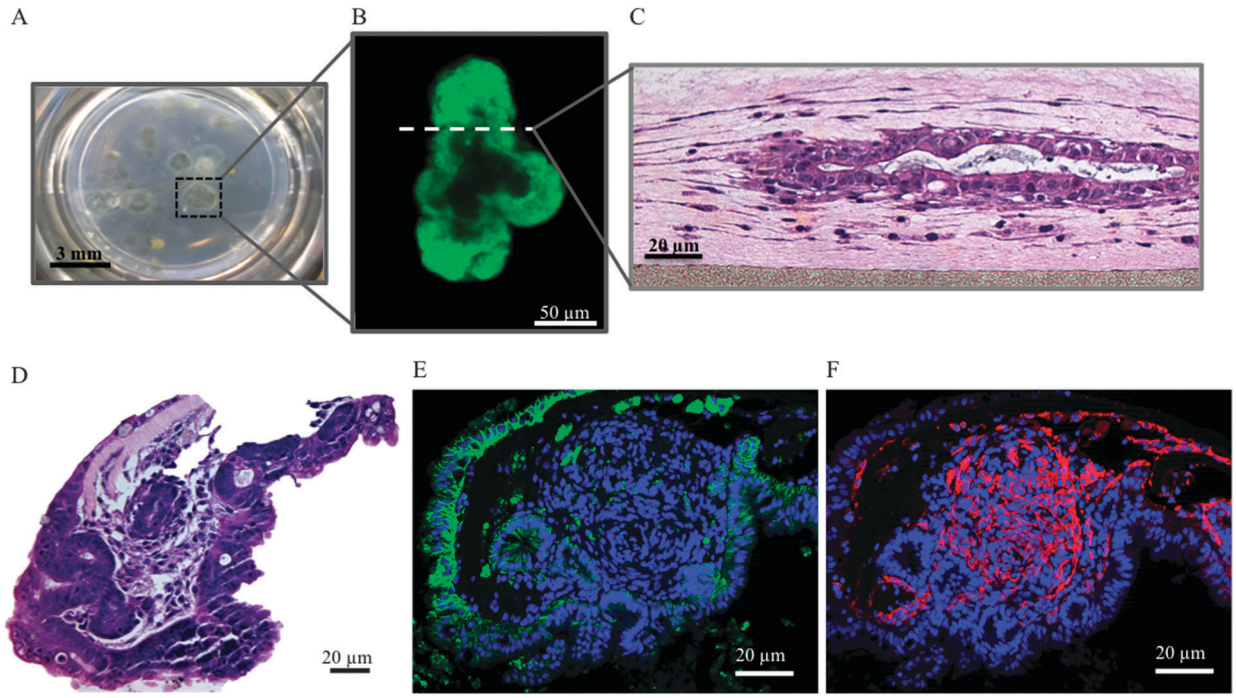

Fig. 1 (A) A macroscopic view of the extensive growth of primary murine neonatal organoids achieved during long-term culture along with (B) a fluorescence confocal microscopy image of a GFP + organoid culture and (C, D) hematoxylin and eosin, (E) E-cadherin, and (F) α-smooth muscle actin stains.

Because myofibroblasts contain the contractile cellular machinery, we reasoned that this cell type was a requirement for organoid contractility. Despite this alteration in protocol, organoids successfully formed within both culture configurations. After one week of culture, organoids in the air–liquid interface configuration generally appeared spherical and symmetric, and these structures began to exhibit bud-like extensions by two weeks, which is consistent with previous reports.[22] In comparison, organoids cultured in the submerged configuration displayed an elevated presence of crypt-like projections already after one week of culture. These differences declined in magnitude over time as organoid diameter expanded (Fig. 2).

Finite element model of oxygen transport within organoid cultures

One key difference between the previously established organoid culture protocols is the presence of the semi-permeable membrane in the air–liquid interface cultures. We hypothesized that the membrane would result in enhanced oxygen transport relative to the submerged configuration. To better understand the effects of the presence of the semi-permeable membrane on culture oxygenation, finite element analysis was used to model oxygen transport and equilibrium oxygen concentrations for submerged and air–liquid interface cultures when exposed to varying ambient oxygen concentrations (Fig. 3). A normoxic oxygen concentration (20%) was chosen to represent standard incubation procedures, whereas 10% and 1% oxygen were chosen to represent increasing degrees of culture hypoxia.

To experimentally measure transport parameters for use in the finite element model, oxygen transport into nitrogen-purged gels of varying collagen type-I density and cell culture media were measured using a commercially available well-plate embedded with oxygen sensors. Oxygen transport through polystyrene surfaces was assumed to be negligible, and a partition coefficient of 1.047×10^{-3} mol (L atm)$^{-1}$ was assumed at the air–liquid interface.[27,28] Diffusion coefficients were measured to be 2.0×10^{-9} m^2 s^{-1} in collagen and 9.0×10^{-9} m^2 s^{-1} in liquid media (Fig. S1A, ESI†). These values are similar in magnitude to those previously reported.[27,29,30] To model oxygen transport in air–liquid interface cultures through the semi-permeable membrane of the transwell inserts, a stiff-spring constant model was utilized to impose a constant flux restriction[27] with a partition coefficient of 0.7, which is based on the experimental membrane porosity as reported by the manufacturer.

We chose to construct a two-dimensional computational model of experimental culture conditions, which assumes that the cultures have radial symmetry. Because the minced explants are randomly seeded into isotropic collagen gels, this is a reasonable assumption. Based on our experimental seeding density and manual counts of the number of organoids in each culture, we calculated a linear density of 5.2 organoids across the culture cross-section. Therefore, we chose to position 5 organoids within the computational model cross-section. A range of organoid sizes was selected for the computational model (250 μm, 350 μm, and 400 μm) to reflect the experimentally observed organoid sizes between 1 day and 1 week of culture (Fig. 2). For simplicity, these organoids were symmetrically arranged along the *x*-axis of the computational model (Fig. 3).

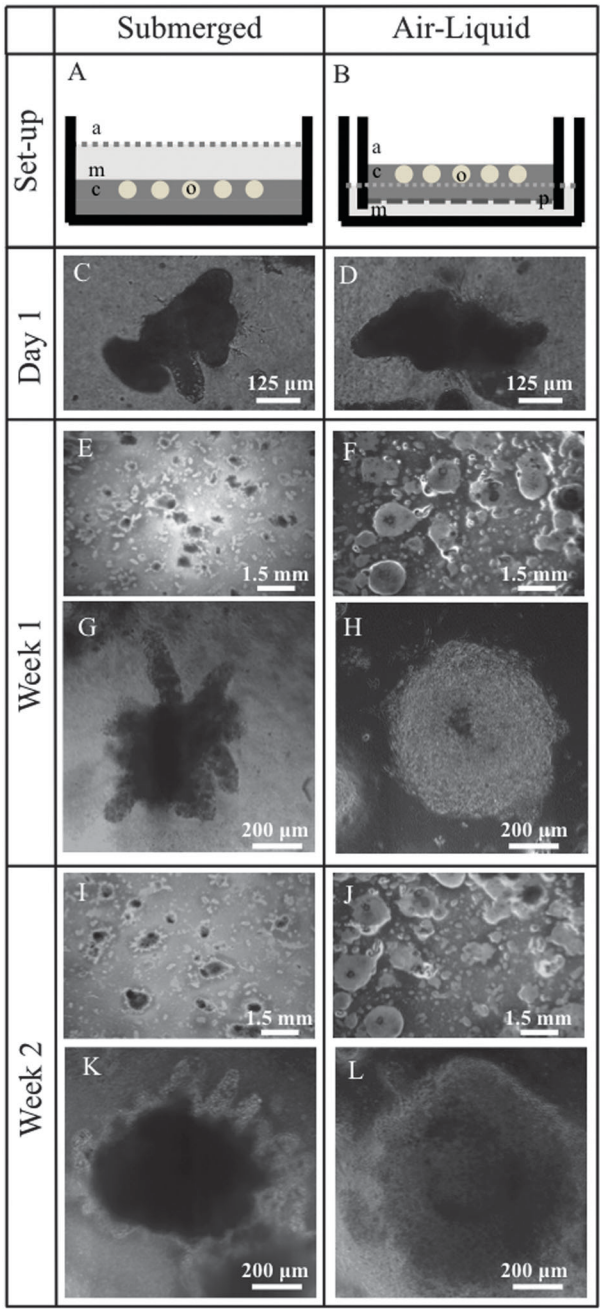

Fig. 2 Schematic of (A) submerged and (B) air–liquid interface culture configurations in which "a" indicates air, "m" indicates culture medium, "c" indicates the encapsulating collagen matrix, "p" indicates the porous membrane, and "o" indicates the primary intestinal organoid. Bright field images of varying magnification are shown after (C, D) one day, (E–H), one week, and (I–L) two weeks of culture.

Organoid consumption of oxygen was modeled using a previously derived expression that follows a Michaelis–Menten type rate:[27,31,32]

$$R_c = R_{max}\left(\frac{c^n}{c^n + C_{MMO_2}^n}\right)\cdot\delta(c > C_{cr}),$$

where R_c is the rate of consumption, R_{max} is the maximum oxygen consumption rate, c is the oxygen concentration [moles m^{-3}], n is a constant with value 1 since the oxygen consumption is a non-cooperative reaction, C_{MMO_2} is a Michaelis–Menten constant corresponding to the oxygen concentration where consumption drops to 50% of its maximum, and δ is a step-down function to account for ceasing of oxygen consumption when c becomes less than C_{cr}, the critical oxygen concentration below which tissue death is assumed to occur after long exposure. To determine R_{max}, organoids were cultured for one week in oxygen-sensing well-plates under normoxic conditions. The experimentally measured equilibrium oxygen concentration at the bottom of the well-plate (*i.e.*, beneath the cultured organoids and directly above the oxygen sensors) was found to be 0.1775 moles m^{-3}. This value is two orders of magnitude larger than the literature-reported value for C_{MMO_2} of 1.0×10^{-3} moles m^{-3}; this confirms that the system is within the oxygen saturation regime for these culture conditions. Incorporating the equilibrium oxygen concentration into our finite element model of oxygen transport yielded a maximum oxygen consumption rate of 0.0006 moles m^{-3} s^{-1} (Fig. S1B, ESI†). This R_{max} value is intermediate between values previously reported for human lung and intestinal epithelial cells and pancreatic islet clusters cultured *in vitro*.[27,33] Finally, the critical oxygen concentration to maintain cell viability, C_{cr}, was chosen to be 1.0×10^{-4} moles m^{-3} based on previously reported literature values.[27,31]

Computationally predicted oxygen transport within organoid cultures

Using the finite element model described above, simulations were run with initial ambient oxygen concentrations of 0.20900, 0.10450, or 0.01045 moles m^{-3} (corresponding to 20%, 10%, or 1% oxygen at 37 °C and atmospheric pressure) for both submerged (SUB) and air–liquid interface (ALI) cultures until reaching equilibrium oxygen concentrations (Fig. 3A–H). All submerged cultures were always predicted to result in lower oxygen concentrations at the organoid surfaces relative to the air–liquid interface cultures (Fig. 3I and Fig. S2, ESI†). This is because oxygen transport in submerged cultures only occurs through the top surface of the liquid medium due to the relative impermeability of oxygen through polystyrene culture dishes (Fig. 3A, C, E and G). In contrast, air–liquid interface cultures enable more uniform and higher oxygen concentrations due to enhanced oxygen transport both from the top air–collagen interface and the bottom semi-permeable membrane interface (Fig. 3B, D, F and H). For example, under 1% ambient oxygen, submerged organoids obtain oxygenation levels that are roughly 61% of those within air–liquid interface cultures (0.0019 *vs.* 0.0031 moles m^{-3}), whereas under normoxia, submerged cultures reach 97% of the oxygen availability that is present in air–liquid interface cultures (0.194 *vs.* 0.199 moles m^{-3}).

As suggested by quasi uni-directional oxygen flux in the submerged cultures (top-down oxygen transport only) *versus* bi-directional flux in air–liquid interface cultures (top-down as well as bottom-up transport), organoids encapsulated in submerged cultures experience significantly higher oxygen gradients than those in air–liquid interface cultures (Fig. 3J). Our model predicts that across an organoid body diameter of

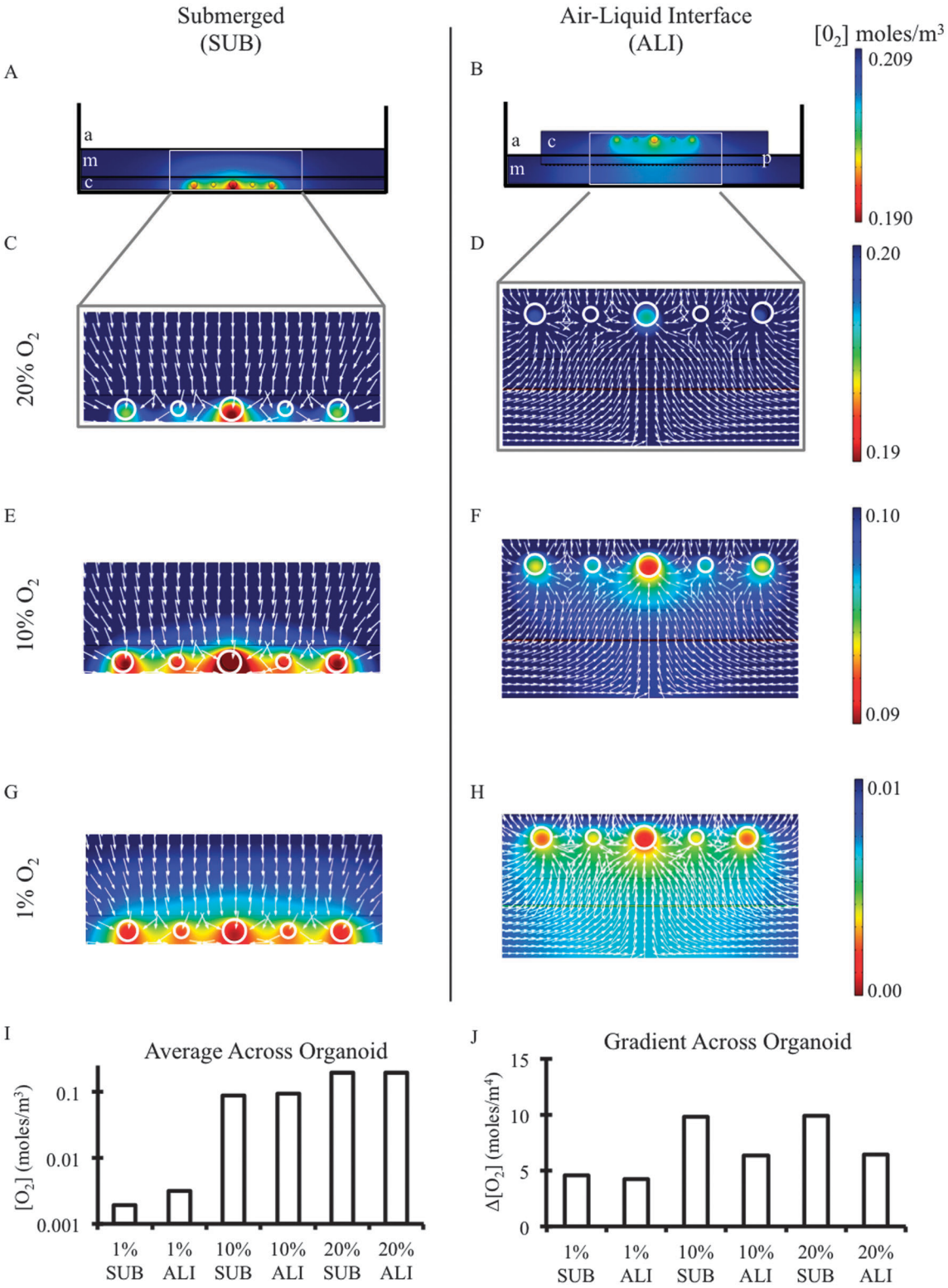

Fig. 3 Finite element simulations of (A, B) equilibrium oxygen concentrations of submerged and air–liquid interface culture configurations under normoxic conditions in which ''a'' indicates air, ''m'' indicates culture medium, ''c'' indicates the encapsulating collagen matrix, ''p'' indicates the porous membrane, and ''o'' indicates the primary intestinal organoid. (C, D) Detailed oxygen concentrations and oxygen flux lines (white arrows) of inset areas from panel A along with similar regions under (E, F) 10% and (G, H) 1% ambient oxygen concentrations. (I) Equilibrium oxygen concentrations and (J) oxygen gradients experienced across the diameter of an encapsulated organoid within submerged and air–liquid interface culture conditions under ambient oxygen concentrations tested.

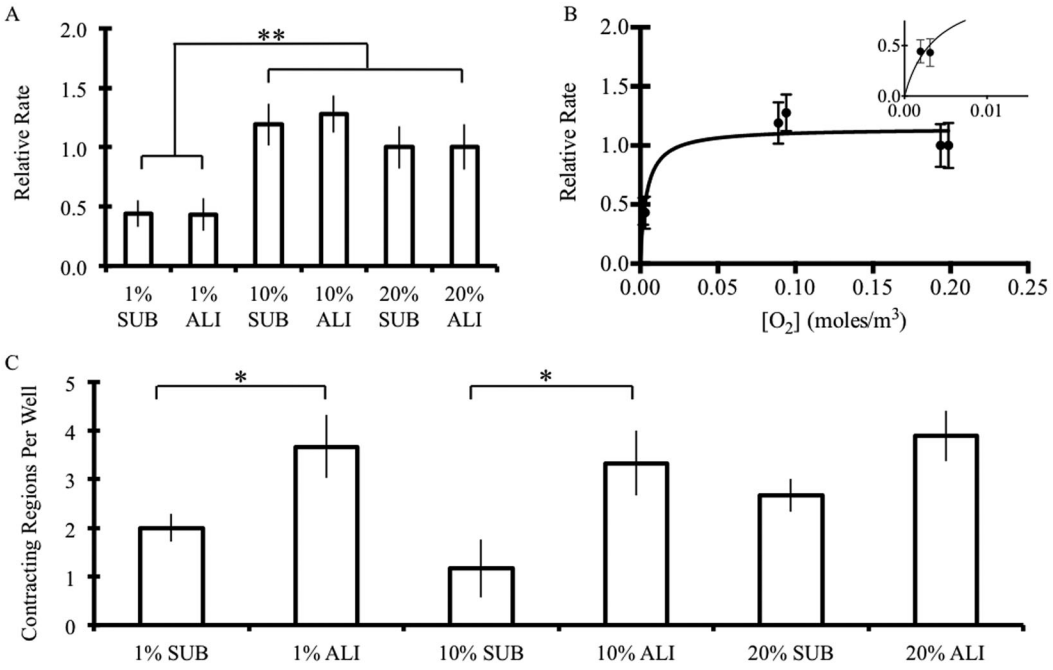

Fig. 4 (A) The relative contraction rate (normalized to 20% ALI condition for each bulk animal harvest) of organoids that demonstrated contractile behavior within submerged and air–liquid interface culture conditions under 1%, 10%, and 20% ambient oxygen for two weeks. When analyzed with respect to predicted equilibrium oxygen concentration, (B) contraction rate was found to have a plateau dependency, demonstrating a steep increase with increasing oxygen availability at low oxygen concentrations and a plateau above roughly 3% oxygen. ** denotes statistical significance, $p < 0.01$. Fit shown is that of concentration-based saturation (contraction rate = $(X \times [O_2])/(Y + [O_2])$, where X and Y are constants). (C) The number of contracting regions per 24-well is shown for submerged and air–liquid interface cultures under 1%, 10%, and 20% ambient oxygen for two weeks. Values shown are mean ± standard error of the mean. * denotes statistical significance, $p < 0.05$. A minimum of 60 organoids were analyzed per condition.

400 μm, the oxygen gradient experienced within submerged cultures is approximately 1.5 times that experienced within air–liquid interface cultures. This difference in oxygen gradient becomes less pronounced under severely hypoxic conditions (1% O_2). This is due to the fact that our model accounts for an oxygen-limited decrease in metabolic activity under extremely oxygen-limited conditions. This is a necessary condition for modeling physiologically relevant cell behavior and adaptation to severely hypoxic settings.[27,31,32]

Lastly, we performed finite element analysis on both submerged and air–liquid interface cultures in the presence and absence of an acellular collagen layer beneath the organoid cultures (Fig. S3, ESI†). This acellular layer is frequently used in air–liquid interface cultures to increase the total height of the culture so that it is not beneath the surface of the liquid medium.[22] Our model predicts minimal change in equilibrium oxygen concentration or oxygen gradient due to the presence or absence of the acellular layer in either submerged or air–liquid interface culture configurations under normoxic conditions (Fig. S3, ESI†).

Influence of oxygenation and oxygen transport on contractile behavior of intestinal organoids

Experimental differences in contractility were then assessed between submerged and air–liquid interface cultures under 1%, 10%, and 20% ambient oxygen concentrations after 2 weeks of culture. Though the maximum contraction rate was found to vary between animal harvests (ranging from 14.3 ± 2.5 to 25.3 ± 1.7 min^{-1}, Video S1–S3, ESI†), normalizing the measured contraction rate to that achieved under 20% air–liquid interface configuration for each harvest enabled us to compare trends across various repeat experiments. The relative contraction rate within any given harvest was significantly influenced by the ambient oxygen concentration, demonstrating a saturation-like dependency on average oxygen concentration across the organoid body (contraction rate = $(X \times [O_2])/(Y + [O_2])$, where X and Y are constants) (Fig. 4A and B). Furthermore, this relationship was shown to plateau to the maximum value at fairly low oxygen concentrations (roughly 3%), suggesting that the contraction rate is only diminished when oxygen is drastically limited (Fig. 4B).

We then quantified the number of distinct contracting regions within a given culture. For both 1% and 10% O_2 conditions, the air–liquid interface culture set-up was found to significantly increase the number of contracting regions within each sample (Fig. 4C) (2.0 ± 0.3 *vs.* 3.7 ± 0.6 and 1.2 ± 0.6 *vs.* 3.3 ± 0.7 for 1% and 10% O_2, respectively, within 24-well-plate cultures). This increase was also observed under normoxic conditions but not found to be statistically significant (2.7 ± 0.3 *vs.* 3.9 ± 0.5) (student's T test, $p < 0.05$).

Influence of exogenous R-spondin1 on contractile behavior of intestinal organoids

Given the previously reported importance of Wnt signaling in the development of intestinal tissues both *in vitro* and *in vivo*,[22,23,34–38] we next assessed the ability of exogenous R-spondin-1 (R-spo1),

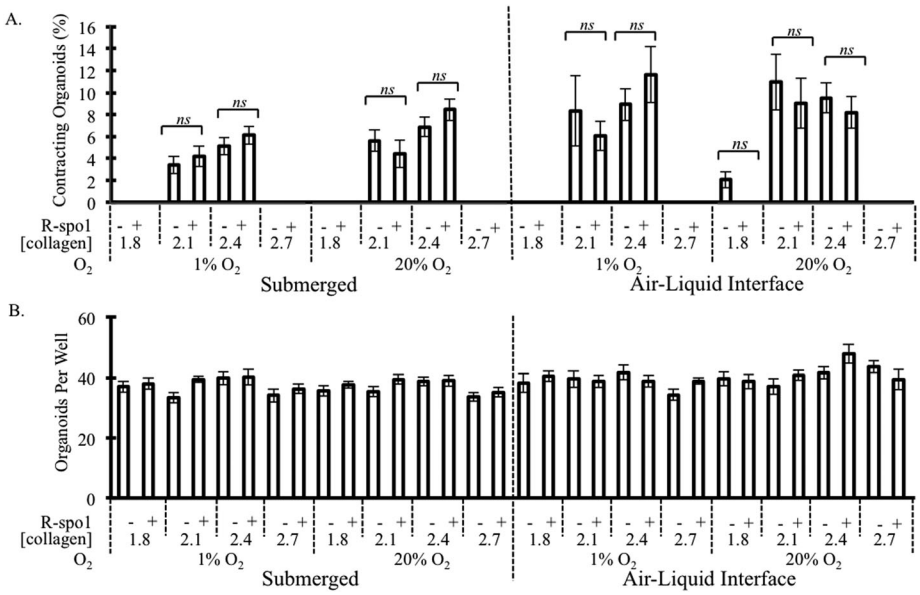

Fig. 5 (A) Percentage of encapsulated organoids per well that demonstrated contractile behavior and (B) total organoid count per well when cultured within either submerged or air–liquid interface cultures under severely hypoxic (1%) or normoxic (20%) conditions for two weeks. Organoids were encapsulated within matrices of type-I collagen densities ranging from 1.8 to 2.7 mg mL^{-1} in the presence or absence of exogenous R-spondin1 (R-spo1). Statistical significance of data comparing cultures with and without exogenous R-spo1 was analyzed by ANOVA and Kruskal–Wallis test ($p < 0.01$, *n.s.* = not significant) and is displayed as mean ± standard error of the mean. A minimum of 300 organoids were analyzed per condition.

a Wnt activating molecule, to enable contraction of organoid cultures. We simultaneously evaluated a range of collagen type-I matrix densities, since matrix properties are well known to affect several other types of contractile cultures including skeletal myoblasts and cardiomyoblasts.[39,40] When all variables are analyzed independently, it can be readily observed that the addition of R-spo1 had no effect on the contractility of these neonatal murine primary organoids (Fig. 5A), despite the demonstrated activity of this recombinant molecule (Fig. S4, ESI†).[38] After two weeks of cultures, no statistically significant differences in the percentage of contracting organoids were found between samples that received exogenous R-spo1 and those that did not regardless of collagen concentration, culture configuration, or ambient oxygen concentration. Importantly, no statistically significant differences were found in the total number of organoids across all culture conditions, suggesting that neonatal primary murine intestinal organoids can be successfully maintained within all of the culture conditions tested (Fig. 5B).

Influence of matrix density on contractile behavior of intestinal organoids

Strikingly, contraction was only observed within intermediate concentrations of bovine collagen type-I (2.1 and 2.4 mg mL^{-1}, Fig. 5A). Contraction was almost never seen in 1.8 mg mL^{-1} or 2.7 mg mL^{-1} collagen matrices. The single exception was the minimal contraction seen in air–liquid interface cultures within 1.8 mg mL^{-1} collagen under normoxic conditions without R-spondin1; however, this frequency value, 2.06%, was significantly lower than that seen within 2.1 and 2.4 mg mL^{-1} matrices at the same oxygen conditions without R-spo1, 10.96% and 9.52%, respectively, and was found to be not significantly different than the populations that were not contracting (Kruskal–Wallis test, $p < 0.05$). When all variables are analyzed independently, no statistically significant differences in contractility were found between organoids encapsulated in 2.1 mg mL^{-1} collagen and those in 2.4 mg mL^{-1} collagen.

Given the profound impact of collagen matrix density on the onset of organoid contractility, further materials characterization of the collagen matrices was performed. Scanning electron microscopy (SEM) was used to assess differences in matrix morphology as a function of collagen density (Fig. 6A and Fig. S5, ESI†). Void space, defined as total area unoccupied by collagen fibers, was found to generally decrease as collagen concentration increased, with values of 36.6% (±4.69%), 21.1% (±2.00%), 23.4% (±4.60%), and 7.76% (±5.7%) reported for 1.8, 2.1, 2.4, and 2.7 mg mL^{-1} matrices, respectively (Fig. 6B). Conversely, fiber bundle thickness was found to generally increase as collagen concentration increased (Fig. S6A, ESI†). The intermediate collagen densities of 2.1 mg mL^{-1} and 2.4 mg mL^{-1} showed no statistically significant differences in void space percentage or fiber bundle thickness. When the percentage of contracting organoids is plotted with respect to void space, it is observed that there is a narrow range of matrix morphology (~22% void space) over which contractility occurred (Fig. 6C).

Oscillatory rheology was utilized to study the mechanical differences between the matrices. Storage moduli and crossover frequencies were determined by evaluating the plateau regions of oscillatory frequency sweep data (Fig. S6B, ESI†). Overall, storage modulus was shown to increase as collagen density increased, with values of 10.3 Pa (±2.61 Pa), 28.6 Pa (±4.32 Pa),

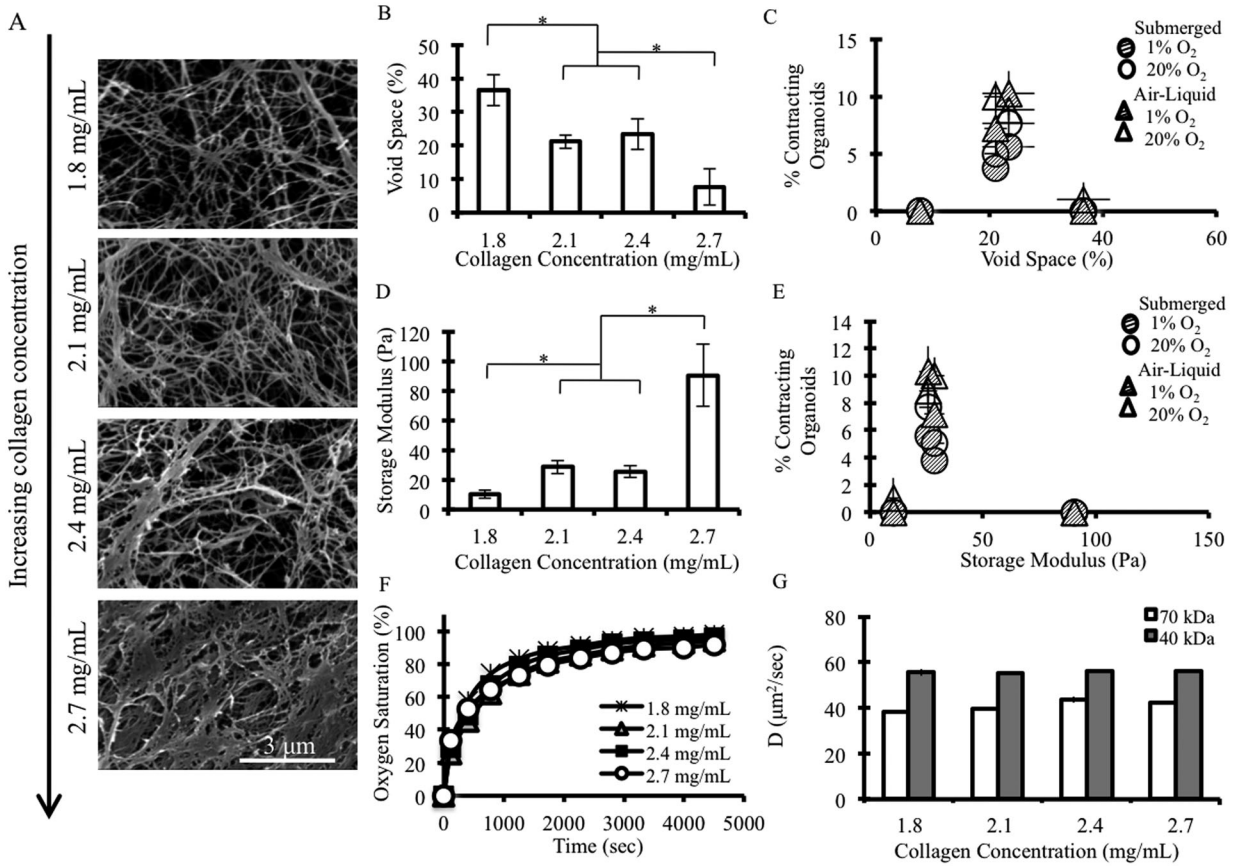

Fig. 6 (A) Characteristic scanning electron micrographs of bovine collagen type-I matrices of varying density. (B) Matrix void space was found to decrease at higher collagen densities and (C) to correlate with contractility for all culture configurations and ambient oxygen conditions tested. (D) Storage modulus was found to increase with collagen density and (E) to correlate with contractility for all culture configurations and ambient oxygen conditions tested. (F) Oxygen transport and (G) diffusion coefficients of 40 and 70 kDa FITC–dextran molecules were not found to differ amongst hydrated collagen gels of varying densities. * denotes statistical significance, student's T test, $p < 0.01$.

25.7 Pa (±4.02 Pa), and 90.65 Pa (±21.3 Pa) reported for 1.8, 2.1, 2.4, and 2.7 mg mL^{-1} matrices, respectively (Fig. 6D). Crossover frequency was also shown to generally increase as collagen density increased (Fig. S6C, ESI†). The intermediate collagen densities of 2.1 mg mL^{-1} and 2.4 mg mL^{-1} showed no statistically significant differences in storage moduli or crossover frequencies. When the percentage of contracting organoids is plotted with respect to storage modulus, it can be seen that there is a narrow range of matrix mechanical properties ($G' \sim 27$ Pa) over which contractility occurred (Fig. 6E).

To investigate any potential differences in nutrient transport that may result from collagen matrix density, the transport of molecules of various sizes was measured within all collagen formulations of interest. As a typical small molecule, oxygen transport was measured using well-plates with embedded oxygen sensors, and transport rates within all matrices shows no statistically significant differences (Fig. 6F). To mimic the transport of larger protein nutrients such as growth factors, we tracked the diffusion of two fluorescently labeled dextran polymer samples (average molecular weights of 40 and 70 kDa) using fluorescence recovery after photobleaching (FRAP). Similar to the oxygen transport results, diffusivity of the larger dextran molecules was not significantly slower in the higher density matrices (Fig. 6G).

Myofibroblast organization and direction of contractile movement

To further understand the contraction of primary intestinal organoids *in vitro*, immunocytochemistry and real-time imaging were used to characterize differences in myofibroblast organization and the directional properties of observed contractile behavior. From this microscopic analysis, two distinct types of contractile movement and myofibroblast organization are clearly observed: (1) longitudinal, in which contractile movement is most prominent along a longitudinal axis (Fig. 7A and B, Video S2, ESI†) and myofibroblasts are highly organized and aligned (Fig. 7C and D), and (2) radial, in which contractile movement is more symmetric (Fig. 7E and F, Video S3, ESI†) and myofibroblasts appear randomly aligned (Fig. 7G and H).

While lower ambient oxygen appeared to favor longitudinal contractions, both longitudinal and radial contractions were observed within 10% and 20% ambient oxygen cultures and in both submerged and air–liquid interface cultures (Fig. 7I and Fig. S6, ESI†). Similarly, lower oxygen concentrations appeared

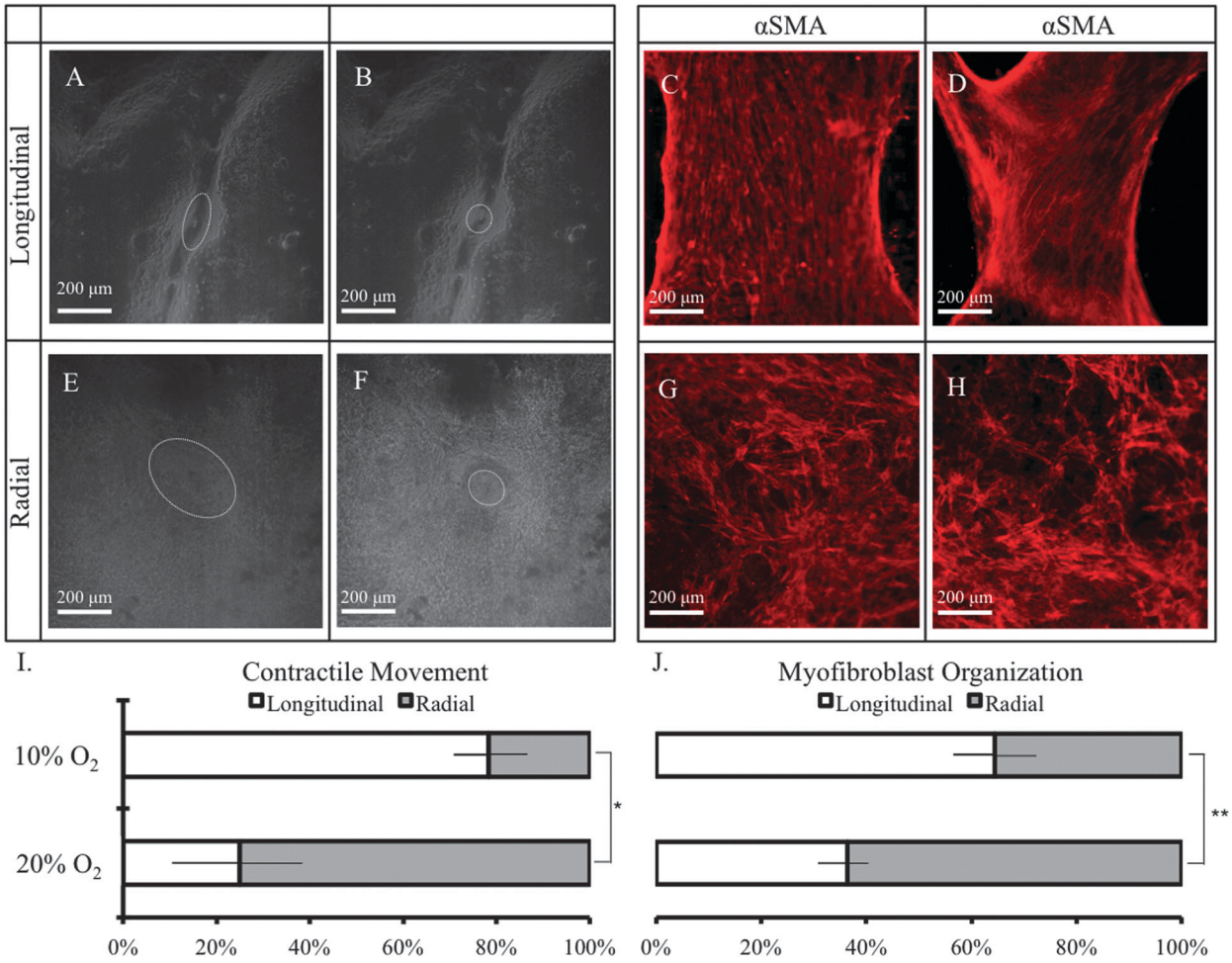

Fig. 7 Assessment of (A–D) longitudinal and (E–H) radial contractile movement and myofibroblast organization at two weeks. Real-time imaging was used to assess contractile behavior. Contracting regions of interest are highlighted with white dashed outlines pre- and post-contraction for ease of viewing (A, B, E, F). Myofibroblast organization is assessed *via* immunocytochemical staining of myofibroblast marker α-smooth muscle actin (C, D, G, H). Percentage of longitudinal or radial directionality of (I) contractile movement and (J) myofibroblast organization surrounding primary organoids under 10% and 20% ambient oxygen concentrations. * denotes statistical significance, $p < 0.05$. ** denotes statistical significance, $p < 0.01$. A minimum of 120 total organoids and 6 contractile organoids were analyzed per condition.

to promote longitudinal myofibroblast morphology (Fig. 7J). As observed in earlier experiments (Fig. 4A and B), the contraction rates at either 10% or 20% ambient oxygen for both submerged and air–liquid interface cultures were similar, regardless of contractile geometry or myofibroblast alignment. No statistically significant differences were found in the direction of contractile movement or myofibroblast organization between cultures in air–liquid interface and submerged configurations (Fig. S7, ESI†).

Influence of culture geometry on contractility

Previously reported organoid cultures have been maintained within a variety of tissue culture devices, ranging from 96-well-plates (~7 mm diameter) to 30 mm transwell inserts, both with and without acellular collagen layers.[22,23] This diversity of culture protocols results in a broad range of encapsulating gel geometries. Given the critical importance of the matrix structure and mechanics in enabling organoid contractility (Fig. 6), we next evaluated whether gel geometry would also impact organoid contractility by creating cultures of identical organoid density but different gel heights and diameters. Interestingly, contraction was only observed within gels of diameter equal to or less than 15.5 mm (Fig. 8A, $n > 60$ organoids per condition). No contraction was seen within cultures with gel diameter greater than or equal to 30 mm. Furthermore, through immunocytochemical staining of α-smooth muscle actin and nuclear DAPI staining, we frequently observed clear attachments of myofibroblast networks to the surrounding edges of the culture wells and inserts (Fig. 8B–F). Similar to contraction, this was only observed within cultures of gel diameters equal to or less than 15.5 mm and was not seen in any of the larger cultures.

Discussion

Air–liquid interface cultures promote contractility of primary intestinal organoids relative to submerged culture configurations

The goal of this work was to identify culture conditions that promote contractility of primary intestinal organoids *in vitro*.

A

Configuration	Well Plate	Culture Volume (μL)	Acellular Volume (μL)	Gel Diameter (mm)	Culture Height (mm)	Acellular Height (mm)	Aspect Ratio (height/width)	Surface Area/ Volume Ratio	Media Volume (μL)	Contraction Observed
ALI	24 well	100	100	12.00	0.88	0.88	0.15	0.33	292	☑ Yes
ALI	24 well	100	0	12.00	0.88	0.00	0.07	0.33	292	
SUB	24 well	100	100	15.50	0.53	0.53	0.07	0.26	292	
SUB	24 well	100	0	15.50	0.53	0.00	0.03	0.26	292	
ALI	6 well	1,000	1,000	30.00	1.42	1.42	0.09	0.13	500	⊘ No
SUB	6 well	1,000	1,000	35.12	1.04	1.04	0.06	0.11	500	

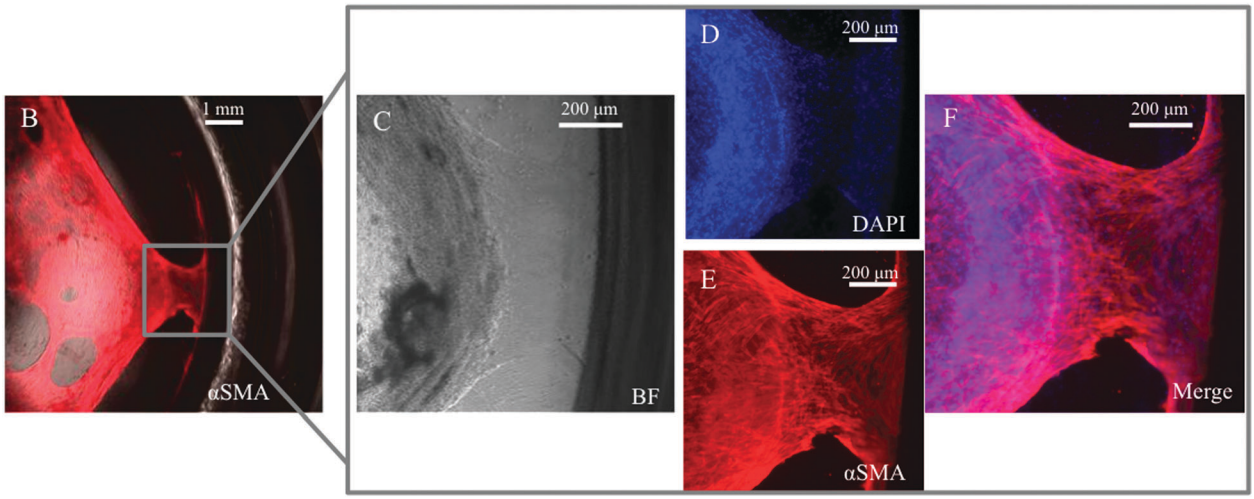

Fig. 8 (A) Table of culture geometries analyzed and instances in which *in vitro* contraction was observed. (B–F) Immunocytochemical staining of α-smooth muscle actin and nuclear DAPI staining demonstrate attachment of intestinal myofibroblast network to surrounding well edges. This observation of myofibroblast anchoring was only seen in cultures with gel diameters equal to or less than 15.5 mm. Similar to contraction, this was not observed in cultures of diameters greater than or equal to 30 mm. A minimum of 60 organoids were analyzed per condition.

The air–liquid interface culture configuration was found to increase the likelihood of achieving contractile intestinal organoid cultures relative to the submerged configuration (Fig. 4C), regardless of ambient oxygen concentration and despite identical contraction rates (Fig. 4A and B). The choice of submerged *versus* air–liquid interface configuration is likely not impacting overall culture viability, as the number of observed organoids were identical across all culture configurations (Fig. 5B). Though subtle differences in organoid shape were observed after several days of culture, these differences declined over time and were minimal by two weeks, which is when organoid contractility was typically first observed (Fig. 2). Similarly, the myofibroblast organization at two weeks did not appear to be significantly impacted by the culture configuration (Fig. S7, ESI†). When averaged together, air–liquid interface cultures rendered contraction in approximately 10% of organoids within any given sample, a similar reproducibility as that reported for iPSC-derived epithelial-cyst-like structures and smooth muscle sheets.[26] These observations clearly call for further investigation into the potential mechanism (or mechanisms) through which the air–liquid interface configuration promotes intestinal organoid contractility.

Air–liquid interface cultures have enhanced oxygen transport rates, higher equilibrium oxygen concentrations, and decreased oxygen gradients compared to submerged cultures

While conventional submerged culture set-ups are most commonly used for three-dimensional mammalian cell culture, air–liquid interface culture configurations have proven particularly useful in the differentiation and organization of barrier-forming tissues and cell types such as keratinocytes and full-thickness epidermis,[41–46] multilayered corneal tissue,[47] as well as lingual,[48] cervical,[49] and endometrial epithelial cells.[50] Although the specific mechanisms have yet to be fully elucidated, we hypothesized that one key advantage to the "air–liquid interface" is the enhanced oxygen transport that results from exposure of the top of the culture to open-air conditions. Our oxygen transport simulations demonstrate that air–liquid interface cultures are also significantly affected by the presence of an oxygen permeable membrane at the bottom of the culture. This geometric configuration enables oxygen transport both from the top and the bottom of the culture, thereby increasing the overall oxygen concentration and significantly decreasing the oxygen gradient that arises within the culture matrix (Fig. 3). These data suggest that the use of air–liquid interface cultures may be useful for other cell types with particularly high rates of oxygen

consumption or for those that are especially sensitive to hypoxic conditions.

In vivo, the epithelial cells that line the intestinal luminal surface reside in a uniquely steep oxygen gradient naturally.[51] This is because they are located between the predominantly anaerobic intestinal lumen and the highly metabolically active and vascularized lamina propria. Thus, we hypothesized that oxygen gradient may influence contractility of encapsulated organoids. Additionally, intestinal tissue experiences profound fluctuations in oxygenation due to fasting and feeding patterns that alternately recruit 5% to 30% of total blood volume, respectively, to be localized to the intestinal tract.[51] Hypoxic effects on barrier function of both the blood–brain barrier[52] and the luminal surface of the intestine have been studied, the latter demonstrating the existence of adaptive measures to protect barrier function during hypoxia.[53] Based on the unique oxygen environment experienced by intestinal tissue *in vivo*, we hypothesized that high metabolic activity and hence adequate oxygen transport would be necessary for contractile behavior *in vitro*.

Oxygen availability is not the key determinant to promote contractility, although it has a significant impact on contraction rate

Within this study, the utilization of porous membranes was found to be beneficial in promoting contractility in primary organoids, which may be in part due to the enhanced oxygenation that results from the nearly symmetric, multi-directional transport of oxygen. However, even severely hypoxic air–liquid interface cultures had more contracting regions than normoxic submerged cultures (Fig. 4C), despite having overall lower oxygen concentrations in the hypoxic air–liquid interface configuration (Fig. 3). This suggests that, though oxygen concentration and gradient may be mitigating factors, they are not the key determinants in "turning on" contractile behavior.

In contrast, oxygen concentration was found to significantly impact the contraction rate (Fig. 4A and B). Relative organoid contraction rate had a saturation-like dependence on the average oxygen concentration across the organoid body, and was found to quickly level off in non-oxygen-limited conditions (greater than approximately 3% oxygen) (Fig. 4B). This suggests that the rate of contraction, a metabolically taxing process, is responsive to oxygen availability within the culture and therefore potentially sacrificed in oxygen-limited situations. This is an interesting observation considering the range of oxygen concentrations experienced within the digestive tract during feeding and fasting and the respective contractile patterns that are necessary at those times.[51]

The observed maximum organoid contraction rate was found to vary across individual animal harvests (ranging from 14.3 ± 2.5 to 25.3 ± 1.7 min^{-1}). This variation may be due to various contributing factors, such as the precise age of the neonatal mouse, the time between animal sacrifice and tissue harvesting, and the duration of the harvest and seeding process prior to the administration of nutrients. Because of this harvest-based variability, we chose to normalize the measured contraction rates to the rate obtained within normoxic air–liquid interface cultures within any given bulk animal harvest, in which tissue from all siblings sacrificed was homogeneously mixed prior to seeding. This normalization enabled comparison across various harvests and culture attempts. Additionally, for non-oxygen-limited cultures, the absolute contraction rates measured were similar in magnitude to those reported for healthy longitudinal gastrointestinal muscle ($\sim$37 cycles per minute),[54] further emphasizing that these culture conditions enable the recapitulation of a physiologically-relevant behavior pattern *in vitro*.

Oxygen concentration impacts myofibroblast organization and orientation of contractile movement

In addition to its effects on contraction rate, oxygen concentration was also found to impact the orientation of contractile movement (Fig. 7I) and the underlying myofibroblast organization (Fig. 7J). As organoid contraction has only been reported thus far for cultures containing myofibroblasts as well as epithelial cells,[22] the intestinal organoids studied in this work are a three-dimensional co-culture system of these two predominant cell types. Thus, the organoids consist of an epithelial monolayer surrounding an enclosed lumen as well as a peripheral network of stromal intestinal myofibroblasts that extend outward from the organoid core (Fig. 1C–F) along with minor numbers of other resident cell types, which may include smooth muscle, neuronal, immune, and endothelial cells.[22] During intestinal organoid development, the stromal myofibroblast population reorganizes to form an extended network around the epithelial core.[22] The muscle-like contractions of these "myo"-fibroblasts are thought to be physically responsible for the contractile motion of intestinal organoids *in vitro*.[22] Furthermore, it is reasonable to assume that in order for contraction to occur many cells need to spatially organize and form sufficient mechanical connections in order to propagate a substantial force; therefore, we hypothesized that myofibroblast organization may be directly linked to contractile behavior *in vitro*.

Our observations suggest that there is a correlation between myofibroblast organization and the direction of contractile movement within primary organoid cultures (Fig. 7I and J). Notably, oxygen concentration was found to have a significant effect on both of these factors. Lower oxygen concentrations appear to favor both longitudinal organization and longitudinal contractile movement, whereas higher oxygen availability results in higher radial organization and movement. It is interesting to note that two distinct contractile movements occur within the intestine *in vivo*: segmentation and peristalsis, which occur during normal digestive cycles and within discrete layers of intestinal tissue. These data demonstrate that merely recording the percentage of contracting organoids or the contraction rate is not enough to fully capture the subtle differences that may exist in the character of the contractile movement *in vitro*.

Exogenous R-spondin1 does not enhance contractility of primary murine neonatal intestinal organoids

Wnt signaling is hypothesized to play a key role in determining stem cell fate, maintaining intestinal homeostasis, and influencing organoid development.[22,34] The inhibition of Wnt signaling results in the loss of intestinal cell proliferation, depletion of secretory lineages, and widespread architectural degeneration

of intestinal crypts.[35,36] Activated Wnt signaling through R-spondin1 has been reported to result in enhanced proliferation of intestinal cells *in vivo*[37,38] and enhanced outgrowth of organoid cultures *in vitro*.[22,23] Based on these data, we hypothesized that inclusion of R-spondin1 within our engineered microenvironments may enhance organoid survival and contractility. However, for these neonatal murine intestinal organoids, addition of exogenous R-spondin1 was found to have no significant effect on the viability of organoids out to 14 days of culture, regardless of encapsulating matrix density, culture configuration, or ambient oxygen concentration (Fig. 5B). Similarly, the addition of R-spondin1 was found to have no significant effect on organoid contractility (Fig. 5A). These data are consistent with the idea that intestinal myofibroblasts rather than intestinal epithelial cells, which are thought to be the main target of R-spondin1, are the key regulators of contractility. However, it remains possible that exogenous Wnt signaling may improve the viability or contractility of adult murine or human organoid cultures and should therefore be studied further within those systems.

Encapsulating matrix density serves as a "permissive switch" that enables contractile behavior to occur in primary intestinal organoid cultures

Matrix morphology and matrix mechanical properties can have pronounced effects on several cellular processes including adhesion, spreading, migration, and proliferation.[55,56] Therefore, changes in collagen density have the potential to produce profound effects on the outgrowth and self-organization of encapsulated three-dimensional cultures. For example, changes in collagen matrix density have been shown to influence the density, cross-sectional area, and path-finding abilities of endothelial cell-derived vessels *in vitro*[57–59] and *in vivo*.[60] Furthermore, the often fibrillar structure of collagen gels in combination with the air–liquid interface culture configuration has been hypothesized to promote the close-packing of cells, an effect that is thought to be advantageous to barrier-forming cell types, such as those that populate the epithelial lining of the intestine.[41,61] Based on these data, we hypothesized that variations in collagen matrix density would result in altered ability of organoids to expand, self-organize, and contract within the surrounding matrix. Indeed, matrix density was found to be a key determinant in promoting contractile behavior in primary intestinal organoids. Contractile behavior was exclusively observed within a narrow range of collagen type-I densities (Fig. 5A). This suggests that matrix density acts as a "permissive switch" to enable contractile behavior *in vitro*.

As many matrix properties will change as a result of changing matrix density, including mechanics, porosity, transport rates, and cell-adhesive ligand concentration, any one or a combination of these effects may be responsible for the onset of contractile behavior. To further elucidate the potential mechanisms by which matrix density may promote contractility, we then performed a series of materials characterization studies on the various collagen matrices. As the transport of both small and large molecules (molecular weights spanning 32 to 70 000 g mol^{-1}) was unaffected by collagen hydrogel density (Fig. 6F and G), this "permissive switch" is not a consequence of differences in nutrient or signaling molecule diffusion. Furthermore, functional contraction was shown to occur equally within both the 2.1 and 2.4 mg mL^{-1} collagen matrices. As these two matrix densities resulted in indistinguishable organoid behavior, our data suggests that this "permissive switch" is not due to differences in the density of cell-binding domains, heparin-binding domains, or other bioactive sequences within the collagen that are directly altered by collagen concentration.

Matrix structure and mechanics may promote the organization of contractile networks of intestinal myofibroblasts

Organoid contraction was only observed within matrices with collagen densities of 2.1 and 2.4 mg mL^{-1}. For these two matrices, no statistically significant differences were found in either matrix morphology or mechanical properties (Fig. 6B and D and Fig. S5A and C, ESI†). These data suggest that a narrow range of matrix structure ($\sim$22% porosity) and stiffness (storage modulus of roughly 27 Pa) are required to enable primary organoid contractions (Fig. 6C and E). Though rare instances of contraction were seen in a few select samples below this optimal collagen density range (Fig. 5A and 7 contractile organoids out of 356 total encapsulated under identical conditions), this may be due to inhomogeneity in the hydrogel network, resulting in isolated regions of higher collagen density within the gel that would thereby enable organoid contraction. Interestingly, the matrix stiffness that produced the most contractions in our cultures ($\sim$27 Pa) is several orders of magnitude less than that reported for mature, adult intestinal tissue (150–500 kPa).[62–64]

Our experimental observations suggest that the encapsulating matrix must fulfill certain mechanical and/or morphological requirements to enable primary organoid contractility. The matrix must be able to elastically deform and recover in response to the tensile forces exerted by the contracting organoids over many repeated cycles. Additionally, the morphology of the encapsulating matrix must physically present sufficient attachment sites to facilitate robust cellular adhesion yet still provide enough void space for cellular proliferation, migration, and organization to enable organoid development.[65] Lastly, as bulk contraction is likely to be dependent upon the coordinated motion of many myofibroblasts, this process could be assisted by the propagation of forces along the observed collagen fiber bundles.[66–68] As matrix morphology and mechanics will continuously change over time in response to cellular remodeling, future investigation of these microenvironmental cues may benefit from the use of non-destructive imaging methods that can track matrix dynamics.[69–77]

During microscopic observation of contractile cultures, it also became apparent that multi-cellular myofibroblast networks were frequently organized into robust attachments at the interface between the compliant collagen matrix and the rigid culture well and/or insert edges (Fig. 8B–F). These multi-cellular structures were never observed under culture conditions within which contraction did not occur. These data suggest that the interfacial myofibroblast networks may serve as anchorage points that enable more efficient force propagation and hence generation of bulk contractions. Consistent with this idea, we observed that the ability to contract was seemingly lost in large diameter

cultures, which have much smaller interfacial surface areas relative to the entire culture volume (Fig. 8A). We hypothesize that increasing the interfacial surface area relative to the culture volume will increase the number of cell-interface contacts, thereby increasing the likelihood to form these multicellular myofibroblast anchorage points. In fact, similar to contraction, these prominent myofibroblast anchorage points were also not observed within large diameter cultures. Furthermore, this may help to explain the enhanced contractility observed within air–liquid interface cultures, which have an inherently smaller diameter due to the presence of the rigid transwell insert within the culture well. Taken together, these data suggest that spatial geometry and mechanics of the culture microenvironment, which includes both the encapsulating matrix as well as the surrounding tissue culture device, may be key determinants of intestinal organoid functionality. This hypothesis merits further experimental and theoretical analysis through systematic alteration of microenvironmental cues.

Experimental

Intestinal organoid culture setup and conditions

Experiments were performed in accordance with APLAC regulations and under Stanford University approved protocols. Actin-GFP C57BL/6 or wild-type C57BL/6J neonatal mice were used to generate intestinal organoids following previously described methods with modifications.[22] Briefly, 5 cm lengths of small intestine were harvested using aseptic techniques. The intestinal lumen was flushed with ice-cold phosphate buffered saline (PBS) using a fine-gauge syringe needle to remove any residual contents and then opened longitudinally. The tissue was then rinsed three times in sterile, ice-cold PBS and minced rapidly into tissue explants of <1 mm^3 in size using iris scissors. The resulting finely minced tissue explants were immediately mixed in 500 μL bovine tendon type-I collagen (Cellmatrix I-A, Nitta Gelatin, Osaka, Japan) and kept on ice. All tissue-containing collagen aliquots were homogeneously mixed prior to sampling for seeding. The collagen concentrations that were tested ranged from 1.8 to 2.7 mg mL^{-1}. Varying collagen concentrations were achieved by reducing the volume of collagen stock solution (3.0 mg mL^{-1}) and replacing that volume with an equivalent amount of 10× Ham's F12 media (Life Technologies, Carlsbad, CA) without sodium bicarbonate. Reconstitution buffer volumes were kept constant across all conditions (Table 1). Reconstitution buffer was comprised of 2.2 g sodium bicarbonate (Sigma-Aldrich, St. Louis, MO) in 100 mL of 0.05 N NaOH and 200 mM HEPES, prepared according to the manufacturer's instructions. Subsequently, mixtures were put into either submerged or air–liquid interface culture configurations. Final tissue densities are estimated to be 1 cm of minced, explanted tissue per 100 μL of collagen matrix.

For submerged tissue cultures, 100 μL or 1000 μL of the collagen and minced tissue explant mixture was pipetted to the bottom of each well of 24-well or 6-well tissue culture plates, respectively (BD Biosciences, Bedford, MA). In the case of 6-well-plates, this tissue-containing layer was placed on top of a 1000 μL acellular collagen layer that had been given at least 15 minutes to gel prior to the addition. The cultures were all then placed into a 37 °C humidified incubator for 15 minutes to give sufficient time for the tissue-containing collagen to gel, and then 292 μL for 24-well-plates or 500 μL for 6-well-plates of cell culture media were added on top of the culture (Fig. 2A). For air–liquid interface tissue culture setup, similarly, 100 μL or 1000 μL of acellular collagen gel was pipetted to the bottom of a 12 mm or 30 mm diameter transwell insert, respectively, with a 0.4 μm porous polytetrafluoroethylene membrane (Millipore, Billerica, MA). The acellular collagen layer was given at least 15 minutes to gel, after which 100 μL or 1000 μL of the collagen and minced tissue explant mixture was added as a uniform layer above it, depending on the size of the insert. After 15 minutes, 292 μL or 500 μL of cell culture media was added to the outside of the transwell insert for 24-well or 6-well-plates, respectively. This particular volume was calculated so the media height closely matches the height of the acellular collagen gel layer in the transwell insert when placed in between the transwell insert and the sides of the surrounding well.

Cell culture media was composed of Advanced DMEM/F12 (Life Technologies), 10% fetal bovine serum (Life Technologies), 1× penicillin/streptomycin/glutamine (Life Technologies), and 10 mM HEPES. Culture media was prepared with and without 500 ng mL^{-1} R-spo1-Fc, a protein generated through recombinant fusion of R-spondin1 and the fragmented immunoglobulin Fc.[22] Recombinant Rspo1-Fc was generated using a stably transfected mammalian cell line and purified by protein A-agarose affinity column.[22] Intestinal organoid cultures were maintained and grown for 14 days at 37 °C in 5% CO_2 and either 1% or 10% O_2 (SMA-80D tri-gas incubator, Astec Co., Fukuoka, Japan) or 20% O_2. Cell culture media was changed every three days. Prior to media change, cell culture media was preconditioned in the respective incubator for at least 30 minutes for exposure to 1%, 10%, or 20% O_2.

Phase contrast and fluorescence image acquisition with quantitative analyses

Both phase contrast and fluorescence images of intestinal organoids were taken by Zeiss Axiovert 200M fluorescence microscope with 2× and 10× objectives or a Leica TCS SPE

Table 1 Collagen matrix compositions utilized to generate encapsulating matrices

Concentration [mg mL^{-1}]	Collagen stock [μL]	10× Ham's F12 [μL]	Reconstitution buffer [μL]	Collagen : media : buffer ratio
2.7	450	0	50	9 : 0 : 1
2.4	400	50	50	8 : 1 : 1
2.1	350	100	50	7 : 2 : 1
1.8	300	150	50	6 : 3 : 1

confocal microscope with 10× objective. An environmental chamber encasing the microscope stage was used to maintain a humidified 37 °C environment under the respective ambient oxygen conditions, as indicated. Contracting organoids were captured on video by real-time sequential image acquisition using a camera mounted onto the Zeiss Axiovert 200M fluorescence microscope with a 10× objective. Contractions per minute were measured by direct observation through the microscope eyepiece. Real-time image sequences were processed into videos by Quicktime v7.7 (Apple Inc., Cupertino, CA) and ImageJ (National Institutes of Health Freeware).

Simulation of oxygen transport in organoid cultures

Finite element analysis was performed to simulate oxygen transport in the two distinct culture setups. A drawn-to-scale, two-dimensional model was created for each culture setup using COMSOL Multiphysics 4.2 (COMSOL Inc., Burlington, MA). An extra fine mesh of free tetrahedral elements was used to construct the wireframe. The cross-sectional density and size of modeled organoids was chosen to reflect the density and size of experimental cultures, resulting in a symmetric row of 5 organoids (diameters: 350 μm, 250 μm, 400 μm, 250 μm, 350 μm) along the *x*-axis, centered within the tissue-containing collagen layer.

To experimentally determine the oxygen diffusivities in collagen and media, oxygen saturation into vacuum-exposed or nitrogen-purged gels of varying collagen type-I density hydrated with cell culture media were measured with well-plates embedded with fluorescent oxygen sensors (OxoPlates®, PreSens Precision Sensing GmbH, Regensburg, Germany) and a Tecan Safire microplate reader. Oxygen diffusion coefficients were assumed to be similar through cellular tissue and collagen. A partition coefficient of 1.047×10^{-3} mol L^{-1} atm^{-1} was assumed at the air–liquid interface.[27,28] For the air–liquid interface culture, the semi-porous membrane was simulated by a stiff-spring constant model and a partition coefficient of 0.7, which is based on the membrane porosity (70%) as reported by the manufacturer (EMD Millipore, Billerica, MA).

Oxygen consumption was modeled as a Michaelis–Menten type consumption rate:[27,31,32]

$$R_c = R_{max}\left(\frac{c^n}{c^n + C_{MMO_2}^n}\right) \cdot \delta(c > C_{cr}),$$

where R_c is the rate of consumption, R_{max} is the maximum oxygen consumption rate, c is the oxygen concentration [moles m^{-3}], n is a constant with value 1 since the oxygen consumption is a non-cooperative reaction, C_{MMO_2} is a Michaelis–Menten constant corresponding to the oxygen concentration where consumption drops to 50% of its maximum, and δ is a step-down function to account for ceasing of oxygen consumption when c becomes less than C_{cr}, the critical oxygen concentration below which tissue death is assumed to occur after long exposure. C_{MMO_2} and C_{cr} were given as 1.0×10^{-3} moles m^{-3} and 1.0×10^{-4} moles m^{-3}, respectively, based on literature values.[27,31] R_{max} was determined experimentally by measuring the equilibrium oxygen concentration for a submerged intestinal organoid culture with matched tissue density and 20% ambient oxygen concentration within an Oxoplate.

A simulation endpoint of 30 000 seconds was utilized to ensure equilibration, which typically occurred after only 5000 seconds. Heat-map plots were used to depict oxygen concentrations and arrow plots depict the direction of oxygen flux. Equilibrium concentrations at the top and bottom of the centrally located, 400 μm diameter organoid were used to calculate the average oxygen concentration across the organoid body and the oxygen gradient across the organoid body.

Scanning electron microscope matrix characterization and analyses

Matrices of collagen gels at varying density were imaged using scanning electron microscopy (SEM). Gels were sequentially dehydrated in ethanol and critical point dried prior to imaging at 5000, 10 000, and 15 000 magnification (Fig. 6A and Fig. S5, ESI†). Images at 15 000 magnification were analyzed for percent void space by thresholding at a consistent pixel value for all images using ImageJ (National Institutes of Health Freeware). The porosity values were calculated as the area fraction of void space on the thresholded images. The fiber bundle thickness was calculated as an average distance between void spaces of plot profiles from 70 equally spaced horizontal lines drawn across the thresholded images. Four images were analyzed per condition.

Rheological collagen matrix characterization

To characterize the viscoelastic properties of the bovine tendon collagen with concentrations ranging from 1.8 to 2.7 mg mL^{-1}, dynamic oscillatory shear measurements were performed using a 20 mm cone and plate geometry and a Discovery Hybrid Rheometer (TA Instruments, New Castle, DE). A gap height of 28 μm was used to test 50 μL of each sample. A humidity chamber was placed around the samples during testing to prevent dehydration. The lower plate temperature was regulated at 37 °C. Samples were given 15 minutes at 37 °C prior to testing to allow gelation to occur. The storage modulus, G', and crossover frequency were assessed through identification of the plateau region of a frequency sweep, ranging from 0.100 to 100 Hz at 3% strain (Fig. S6B, ESI†). Six samples were tested at each collagen density.

Molecular diffusivity measurements

Diffusivities for 40 kDa and 70 kDa FITC–dextran were measured by fluorescence recovery after photobleaching (FRAP).[78] FITC–dextran was mixed with collagen stock solution at 2 mg mL^{-1}, after which gels of varying collagen density were formed according to the previously described protocol. 100 μm × 100 μm regions were bleached at 100% laser intensity for 30 seconds prior to capturing recovery at 1.365 second imaging intervals for a duration of 2.5 minutes at 18% laser intensity. Open source MATLAB code (http://www.mathworks.com/matlabcentral/fileexchange/29388-frapanalysis) was used for image analysis and diffusivity calculations.

Conclusions

This work demonstrates that *in vitro* oxygen concentration influences primary organoid contraction rate, the spatial orientation of that contractile movement, and the underlying myofibroblast organization. Matrix density was found to serve as a "permissive switch" that enables contraction to occur, as contraction was only observed over a narrow window of matrix structural and mechanical properties. Regardless of ambient oxygen concentration, the air–liquid interface culture configuration promoted an enhanced degree of contraction relative to submerged culture, and there is evidence of a potential geometric effect at play. Overall, this work suggests that the ability to contract *in vitro* is mechanically and structurally governed, whereas the characteristics of that contraction are influenced by oxygen availability. In addition, this work presents a novel and unique variable that merits further attention in efforts focused on engineering a physiologically functional, contractile replacement tissue construct – the spatial geometry of the *in vitro* culture configuration.

Our identification of *in vitro* culture conditions that achieve reproducible intestinal organoid contraction with tunable rate and directionality is a significant step forward in the development of functional *in vitro* intestinal cultures, a necessary tool to drive advancement in drug screening assays, models of intestinal diseases, and the engineering of functional tissue for regenerative medicine therapies.

Acknowledgements

The authors are grateful for support from NIH Transformative R01 DK085720-01 (C.J.K. and S.C.H.), Stanford Children's Hospital Transdisciplinary Initiatives Program Seed Grant (C.J.K. and S.C.H.), NIH DP2 OD006477 (S.C.H.), and NIH/NIDDK Intestinal Stem Cell Consortium 1U01DK085527 (C.J.K.). R.L.D gratefully acknowledges support from the Stanford BioX Graduate Fellowship and the National Science Foundation Graduate Research Fellowship, DEG-1147470. K.S.Y received support from California Institute of Regenerative Medicine MD Scholars Fellowship, NIH/NIDDK K08 DK096048 01 and Burroughs Wellcome Fund Career Award for Medical Scientists. The authors also acknowledge R.A. DiMarco for assistance with image analysis.

References

1 P. W. Wales and E. R. Christison-Lagay, *Semin. Pediatr. Surg.*, 2010, **19**, 3.
2 A. B. R. Thomson, A. Chopra, M. T. Clandinin, H. Clandinin and H. Freeman, *World J. Gastroenterol.*, 2012, **18**, 3353.
3 D. E. Levin and T. C. Grikscheit, *Curr. Opin. Pediatr.*, 2012, **24**, 365.
4 M. K. Chen and E. A. Beierle, *Biomaterials*, 2004, **25**, 1675.
5 A. Perez, T. C. Grikscheit, R. S. Blumberg, S. W. Ashley, J. P. Vacanti and E. E. Whang, *Transplantation*, 2002, **74**, 619.
6 J. Reyes, J. Bueno, S. Kocoshis, M. Green, K. Abu-Elmagd, H. Furukawa, E. M. Barksdale, S. Strom, J. J. Fung, S. Todo, W. Irish and T. E. Starzl, *J. Pediatr. Surg.*, 1998, **33**, 243.
7 D. Grant, K. Abu-Elmagd, J. Reyes, A. Tzakis, A. Langnas, T. Fishbein, O. Goulet, D. Farmer and on behalf of the Intestine Transplant Registry, *Ann. Surg.*, 2005, **241**, 607.
8 K. Abu-Elmagd, J. Reyes, G. Bond, G. Mazariegos, T. Wu, N. Murase, R. Sindhi, D. Martin, J. Colangelo, M. Zak, D. Janson, M. Ezzelarab, I. Dvorchik, M. Parizhskaya, M. Deutsch, A. Demetris, J. Fung and T. E. Starzl, *Ann. Surg.*, 2001, **234**, 404.
9 J. Reyes, G. V. Mazariegos, G. M. D. Bond, M. Green, I. Dvorchik, B. Kosmach-Park and K. Abu-Elmagd, *Pediatr. Transplant.*, 2002, **6**, 193.
10 T. Kato, S. Nishida, N. Mittal, D. Levi, J. Nery, J. Madariaga, J. Thompson, D. Weppler, P. Ruiz and A. Tzakis, *Transplant Proc.*, 2002, **34**, 868.
11 J. S. Scolapio, C. R. Fleming, D. G. Kelly, D. M. Wick and A. R. Zinsmeister, *Mayo Clin. Proc.*, 1999, **74**, 217.
12 E. E. Kobold and A. P. Thal, *Surg., Gynecol. Obstet.*, 1963, **116**, 340.
13 H. B. Binnington, B. A. Siegel, J. M. Kissane and J. L. Ternberg, *J. Pediatr. Surg.*, 1973, **8**, 765.
14 K. D. Lillemoe, W. R. Berry, J. W. Harmon, Y. H. Tai, R. H. Weichbrod and M. A. Cogen, *Surgery*, 1982, **91**, 293.
15 E. Ring-Mrozik, *Z. Kinderchir.*, 1989, **44**, 363.
16 G. S. Evans, N. Flint, A. S. Somers, B. Eyden and C. S. Potten, *J. Cell Sci.*, 1992, **101**, 219.
17 T. Grikscheit, A. Srinivasan and J. P. Vacanti, *J. Pediatr. Surg.*, 2003, **38**, 1305.
18 T. C. Grikscheit, E. R. Ochoa, A. Ramsanahie, E. Alsberg, D. Mooney, E. E. Whang and J. P. Vacanti, *Ann. Surg.*, 2003, **238**, 35.
19 T. C. Grikscheit, J. B. Ogilvie, E. R. Ochoa, E. Alsberg, D. Mooney and J. P. Vacanti, *Surgery*, 2002, **132**, 200.
20 T. C. Grikscheit, A. Siddique, E. R. Ochoa, A. Srinivasan, E. Alsberg, R. A. Hodin and J. P. Vacanti, *Ann. Surg.*, 2004, **240**, 748.
21 T. C. Grikscheit and J. P. Vacanti, *J. Pediatr. Surg.*, 2002, **37**, 277.
22 A. Ootani, X. Li, E. Sangiorgi, Q. T. Ho, H. Ueno, S. Toda, H. Sugihara, K. Fujimoto, I. L. Weissman, M. R. Capecchi and C. J. Kuo, *Nat. Med.*, 2009, **15**, 701.
23 T. Sato, R. G. Vries, H. J. Snippert, M. van de Wetering, N. Barker, D. E. Stange, J. H. van Es, A. Abo, P. Kujala, P. J. Peters and H. Clevers, *Nature*, 2009, **459**, 262.
24 N. de Souza, *Nat. Methods*, 2009, **6**, 481.
25 T. Sato, D. E. Stange, M. Ferrante, R. G. J. Vries, J. H. van Es, S. van den Brink, W. J. van Houdt, A. Pronk, J. van Gorp, P. D. Siersema and H. Clevers, *Gastroenterology*, 2011, **141**, 1762.
26 A. Yoshida, K. Chitcholtan, J. J. Evans, V. Nock and S. W. Beasley, *J. Pediatr. Surg.*, 2012, **47**, 329.
27 P. Buchwald, *Theor. Biol. Med. Modell.*, 2009, **6**, 5.
28 R. Sander, in *NIST Chemistry WebBook, NIST Standard Reference Database*, ed. P. J. Linstrom and W. G. Mallard, National Institute of Standards and Technology, Gaithersburg, MD, 69th edn, 2011.

29 M. Radisic, W. Deen, R. Langer and G. Vunjak-Novakovic, *Am. J. Physiol.: Heart Circ. Physiol.*, 2005, **288**, H1278.
30 W. Hayduk and H. Laudie, *AIChE J.*, 1974, **20**, 611.
31 E. S. Avgoustiniatos and C. K. Colton, *Ann. N. Y. Acad. Sci.*, 1997, **831**, 145.
32 D. F. Wilson, W. L. Rumsey, T. J. Green and J. M. Vanderkooi, *J. Biol. Chem.*, 1988, **263**, 2712.
33 R. Fleischaker, Jr. and A. Sinskey, *Eur. J. Appl. Microbiol. Biotechnol.*, 1981, **12**, 193.
34 E. Sancho, E. Batlle and H. Clevers, *Annu. Rev. Cell Dev. Biol.*, 2004, **20**, 695.
35 F. Kuhnert, C. R. Davis, H.-T. Wang, P. Chu, M. Lee, J. Yuan, R. Nusse and C. J. Kuo, *Proc. Natl. Acad. Sci. U. S. A.*, 2004, **101**, 266.
36 D. Pinto, A. Gregorieff, H. Begthel and H. Clevers, *Genes Dev.*, 2003, **17**, 1709.
37 K. A. Kim, M. Kakitani, J. Zhao, T. Oshima, T. Tang, M. Binnerts, Y. Liu, B. Boyle, E. Park, P. Emtage, W. D. Funk and K. Tomizuka, *Science*, 2005, **309**, 1256.
38 K. S. Yan, L. A. Chia, X. Li, A. Ootani, J. Su, J. Y. Lee, N. Su, Y. Luo, S. C. Heilshorn, M. R. Amieva, E. Sangiorgi, M. R. Capecchi and C. J. Kuo, *Proc. Natl. Acad. Sci. U. S. A.*, 2012, **109**, 466.
39 D. Sengupta, P. Gilbert, K. Johnson, H. M. Blau and S. C. Heilshorn, *Adv. Healthcare Mater.*, 2012, **1**, 785.
40 C. Chung, B. L. Pruitt and S. C. Heilshorn, *Biomater. Sci.*, 2013, **1**, 1082.
41 J. H. Lillie, D. K. MacCallum and A. Jepsen, *J. Invest. Dermatol.*, 1988, **90**, 100.
42 L. I. Bernstam, F. L. Vaughan and I. A. Bernstein, *In Vitro Cell. Dev. Biol.*, 1986, **22**, 695.
43 N. Basset-Séguin, J. F. Culard, C. Kerai, F. Bernard, A. Watrin, J. Demaille and J. J. Guilhou, *Differentiation*, 1990, **44**, 232.
44 L. I. Bernstam, F. L. Vaughan and I. A. Bernstein, *J. Dermatol. Sci.*, 1990, **1**, 173.
45 M. L. Williams, B. E. Brown, D. J. Monger, S. Grayson and P. M. Elias, *J. Cell Physiol.*, 1988, **136**, 103.
46 R. H. Tammi, M. I. Tammi, V. C. Hascall, M. Hogg, S. Pasonen and D. K. MacCallum, *Histochem. Cell Biol.*, 2000, **113**, 265.
47 N. R. Richard, J. A. Anderson, J. L. Weiss and P. S. Binder, *Curr. Eye Res.*, 1991, **10**, 739.
48 J. H. Lillie, D. K. MacCallum and A. Jepsen, *Exp. Cell Res.*, 1980, **125**, 153.
49 M. A. Stanley, in *Culture of Epithelial Cells*, ed. I. Freshney and M. G. Freshney, John Wiley & Sons, New York, NY, 2nd edn, 2002, ch. 5, pp. 137–170.
50 L. Munson, J. E. Wilkinson and D. H. Schlafer, *Cell Tissue Res.*, 1990, **261**, 155.
51 S. P. Colgan and C. T. Taylor, *Nat. Rev. Gastroenterol. Hepatol.*, 2010, **7**, 281.
52 K. Hayashi, S. Nakao, R. Nakaoke, S. Nakagawa, N. Kitagawa and M. Niwa, *Regul. Pept.*, 2004, **123**, 77.
53 G. T. Furuta, J. R. Turner, C. T. Taylor, R. M. Hershberg, K. Comerford, S. Narravula, D. K. Podolsky and S. P. Colgan, *J. Exp. Med.*, 2001, **193**, 1027.
54 G. W. Hennig, M. Costa, B. N. Chen and S. J. Brookes, *J. Physiol.*, 1999, **517**, 575.
55 B. K. Mason, J. P. Califano and C. A. Reinhart-King, in *Engineered Biomaterials in Regenerative Medicine: Novel Techniques for Clinical Applications*, ed. S. K. Bhatia, Springer, New York, NY, 2011, ch. 2, pp. 19–37.
56 F. Grinnell and W. M. Petroll, *Annu. Rev. Cell Dev. Biol.*, 2010, **26**, 335.
57 A. L. Sieminski, R. P. Hebbel and K. J. Gooch, *Exp. Cell Res.*, 2004, **297**, 574.
58 N. Yamamura, R. Sudo, M. Ikeda and K. Tanishita, *Tissue Eng.*, 2007, **13**, 1443.
59 A. Shamloo, H. Xu and S. Heilshorn, *Tissue Eng., Part A*, 2012, **18**, 320.
60 P. J. Critser, S. T. Kreger, S. L. Voytik-Harbin and M. C. Yoder, *Microvasc. Res.*, 2010, **80**, 23.
61 T. Elsdale and J. Bard, *J. Cell Biol.*, 1972, **54**, 626.
62 D. A. K. Watters, A. N. Smith, M. A. Eastwood, K. C. Anderson and R. A. Elton, *Q. J. Exp. Physiol.*, 1985, **70**, 151.
63 R. Roeder, J. Wolfe, N. Lianakis, T. Hinson, L. A. Geddes and J. Obermiller, *J. Biomed. Mater. Res.*, 1999, **47**, 65.
64 Y. Leng, Z. Ding and L. Gong, *Zhongguo Xiufu Chongjian Waike Zazhi*, 2006, **20**, 292.
65 K. Wolf and P. Friedl, *Trends Cell Biol.*, 2011, **21**, 736.
66 S. P. Carey, C. M. Kraning-Rush and C. A. Reinhart-King, *Conf. Proc. IEEE Eng. Med. Biol. Soc.*, 2011, 4333.
67 B. Li, C. Moshfegh, Z. Lin, J. Albuschies and V. Vogel, *Sci. Rep.*, 2013, **3**, 2425.
68 I. Schoen, B. L. Pruitt and V. Vogel, *Annu. Rev. Mater. Res.*, 2013, **43**, 589.
69 W. R. Legant, C. W. Chen and V. Vogel, *Integr. Biol.*, 2012, **4**, 1164.
70 K. E. Kubow, E. Klotzsch, M. L. Smith, D. Gourdon, W. C. Little and V. Vogel, *Integr. Biol.*, 2009, **1**, 635.
71 C. Brackmann, M. Zaborowska, J. Sundberg, P. Gatenholm and A. Enejder, *Tissue Eng., Part C*, 2012, **18**, 227.
72 R. Cicchi, N. Vogler, D. Kapsokalyvas, B. Dietzek, J. Popp and F. S. Pavone, *J. Biophotonics*, 2013, **6**, 129.
73 S. C. Kuo, *Traffic*, 2001, **2**, 757.
74 A. Usman, W. Y. Chiang and H. Masuhara, *Sci. Prog.*, 2013, **96**, 1.
75 A. R. Bausch, F. Ziemann, A. A. Boulbitch, K. Jacobson and E. Sackmann, *Biophys. J.*, 1998, **75**, 2038.
76 N. Wang, J. P. Butler and D. E. Ingber, *Science*, 1993, **260**, 1124.
77 Y. Li, D. Ho, H. Meng, T. R. Chan, B. An, H. Yu, B. Brodsky, A. S. Jun and M. Yu, *Bioconjugate Chem.*, 2013, **24**, 9.
78 P. Jönsson, M. P. Jonsson, J. O. Tegenfeldt and F. Höök, *Biophys. J.*, 2008, **95**, 5334.

